




Assessment of Natural Frequency and Stress Distribution of the Turbine Blade Subjected to Material Abnormality Using Model-Based Analysis

Muhammad Shahid Bashir ¹, Muhammad Usman ^{*2}, Muhammad Yasar Javaid³, Muhammad Ayub ⁴

* Corresponding author Email: muhammadusman3051@gmail.com

1.  ORCID ID 0000-0002-8696-9327
2.  ORCID ID 0000-0002-8875-0791
4.  ORCID ID 0000-0003-3317-1992

¹Department of Mechanical and Aeronautical Engineering, University of Engineering and Technology, Taxila, 47080, Pakistan

^{2,4}Department of Mechanical Engineering, The University of Lahore, Lahore 54000, Pakistan

³Department of Mechanical Engineering Technology Government College University Faisalabad 38000, Pakistan

Abstract

Crack development in gas turbine blades is a vital feature to be regulated in most of the power and aerospace industries since it significantly impacts the turbine blade's natural frequency and stress distribution. Furthermore, the investigation is necessary to extend the turbine's operational life by removing the possibility of resonance. In this regard, a cloud point model for turbine blades is created first, followed by a detailed study to investigate blade crack formation and its impact on natural frequency and stress distribution. The blade's stiffness decrease is accounted for by the slow propagation of material abnormality/crack in ANSYS utilizing five separate models based on the Block Lanczos method. The results are formulated by removing the number of elements in a sequential order (starting from 0 to 4) from the blade model to obtain subsequent natural frequency and stress distribution for ten vibration modes. As the crack propagates, both the natural frequency and the stress concentration decrease. Furthermore, both of these are closely related to the mode of vibrations. Based on the assessment, it is noted that the proposed model analysis gives a viable approach to significantly handle the operational barriers of the gas turbine in the industrial sector.

Keywords: Model Analysis, Turbine Blade, Crack formation, Natural Frequency, Stress Distribution

Nomenclature

CPM	Cloud point model	SC (σ)	Stress concentration (GPa)
ER	Element removed	Subscripts	
FEA	Finite element analysis	Max	Maximum
NF	Natural frequency (Hz)	Avg	Average

1. Introduction

The gas turbine is one of the viable elements of turbo machines nowadays. It is extensively used in power generation and aircraft jet engine industries as well. The operational development pathway of the gas turbine normally comprises efficiency, lifespan, and reliability. Among all the

components of the gas turbine, the blades are considered to be the utmost critical part of operation [1], as their failure drastically affects the overall working capability of the gas turbine [2]. Moreover, blades are usually subjected to high temperature, high pressure, and alternative loadings. Therefore, cracks can easily be initiated under these conditions [3]. The crack initiation critically impacts the

natural frequency of the blade, leading to an imbalance in the rotor, high vibrations, and high resonance stresses [4]. For instance, a gas turbine of 70MW failed due to the formation of carbides by the blade material at high temperatures in the first stage [5].

Moreover, a turbine blade failure was analyzed and it was found that the change in natural frequency was the root cause of the metallurgical defects [6]. Natural frequency estimation is one of the important parameters from the industrial point of view because resonance arises when the forced vibration matches with one of the natural frequencies of the turbine blade. Therefore, the resonance phenomena are highly undesirable in the industrial sector, because it causes a high amplitude of vibration, leading to damage to the turbo machinery [7]. Several reasons can be responsible for blade failure under high rotation speed and higher temperature of a turbine, like fatigue failure, outer damage, inner damage, dovetail corrosion, erosion, oxidation, material behavior, and resonant phenomena [8-10]. Furthermore, a 50 MW class turbine blade failure was reported, due to the crack formation caused by the creep similar to stress corrosion [11].

In another study, it was found that the solid particle erosion wear, fatigue, oxidation of the trailing edge, and corrosion of the surface are the other main factors of gas turbine blades failure, thus thermal barrier coating of ceramic and refractive materials are suggested to increase the durability and efficiency of the turbine blade for the reduction of possible failure [12, 13]. But these thermal barrier coatings on the other side, are reported practically challenging due to their delamination, which is primarily caused by startup, steady, and stop operation in service [14]. Moreover, a nimonic-105 super-alloy turbine blade was investigated, and it was found that the failure of the blade occurs due to the corrosion fatigue at the root of the blades [15]. It was also observed that hot corrosion is proven one of the drastic failure factors for nickel-based alloy, which eventually damages the second-stage blades of the turbine [16].

Moreover, hot corrosion is highly undesirable on the blades of a turbine, to prevent severe fatal failure, which is caused by the oxidation of material at high temperatures [17]. In addition, the evolution of micro cracks on the surface of the blade increases the stress concentration, leading to blade failure [18]. Furthermore, in another study, it was found that the corrosion fatigue crack extremely reduces the life span of the turbine [19]. To avoid such complications in turbo machinery, failure analysis has gotten the attention of many researchers. The crack formation, its effects, and different crack-initiating phenomena on the blade profile are investigated [20, 21]. Moreover, the finite element analysis and dynamic analysis were carried out to highlight and reduce the turbine blade failure factors [22, 23]. Another investigation based on the numerical and experimental results highlights that the FEA method is one of the accurate techniques instead of performing costly and time-consuming experimental model analysis [24].

In another study, the finite element analysis showed that the major reason behind the bucket segmentation is mainly caused by the failure of a major bucket cooling passage [25]. In a study, the natural frequency of the turbine blade was measured at different rotational speeds, highlighting that the estimated natural frequency follows an increasing trend with the increase in the rotational speed [26]. Furthermore, the frequency and amplitude response function of the gas turbine was studied experimentally, and FEA models were developed for both free and clamped vibration conditions. The results showed that the natural frequency achieves maximum value for the bend-twist mode shape [27]. It was further studied that, the nonlinear friction force at the dovetail interface significantly reduces the vibration amplitude, especially at low rotating speed that ultimately lowers the resonant vibration to avoid failure [28]. In addition, the life span, repair, and failure criteria of the first-stage blades were calculated by using a conjugate analysis of heat transfer across the rotor blade. Furthermore, it was studied that,

the highest pressure and temperature are encountered at the first stage of the turbine blades, causing higher stresses [29].

The current study is undertaken to estimate the natural frequency and stress distribution/concentration of the gas turbine using different crack formations (number of elements removed). The extensive simulation analysis is carried out for five different models (considering 10 modes of vibration). Previously, there have been several studies on the change in the material properties, crack generation, and their possible reasons in gas turbine blades. Whereas, this study investigates the behavior of the two pivotal aspects i.e., the natural frequency and stress distribution of the gas turbine owing to the crack generation and its propagation through model-based analysis. This study further highlights the overall comparison of five different models, which ultimately led to the conclusive trend of possible variation (in NF and SC_{Max}) and failure of turbine blades in cycle operation.

2. The model description and methodology of analysis

2.1. Turbine blade model

The study is undertaken to investigate the behavior of the turbine blade in the form of stress distribution and natural frequencies upon different crack formations. In the first step, a cloud-point model of a gas turbine blade is developed to apply the model analysis for the investigation of both natural frequency and stress distribution owing to the crack formation during the working cycle of a gas turbine. The model is then converted into an FEA model using ANSYS as shown in Fig. 1. The element type of Solid-186 is preferred. This 3-D 20-node advanced order solid element exhibits quadratic displacement behavior, hyper flexibility, stress stiffening, versatility, enormous diversion, creep, and huge strain capacities. The blade material properties are further defined for alloy steel as shown in Table. 1. The alloy steel is usually preferred in the industrial sector due to its mechanical, thermal, and corrosion resistance properties.

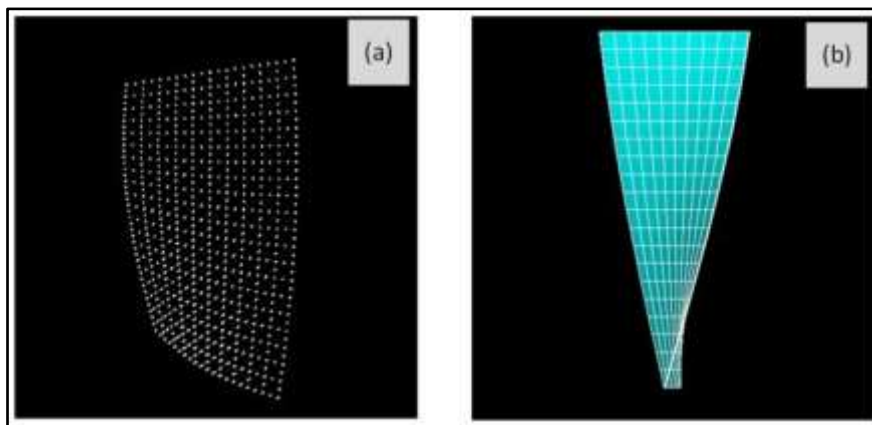


Fig. 1. (a) Isometric view of CPM of a turbine blade, (b) Side view of FEA model of turbine blade

Table 1. Material properties of alloy steel

Material Properties	Value
Mass density [Kg/m ³]	4429
Modulus of Elasticity [GPa]	116
Thermal expansion coefficient [1/K]	1.12×10^{-5}
Poisson' ratio	0.3

As well, in the next step, loads or constraints are defined at the root of the blade at all degrees of freedom. To significantly analyze the impacts of crack formation on natural frequency and stress concentration, the following boundary conditions are applied: one

end of the blade (i.e., the root of the blade) is fixed whereas the tip of the blade is set to free. This means that only constrained loads are taken into account, disregarding the effects of temperature and pressure in the present study. The front view of the turbine blade constrained at the root is shown in Fig. 2.

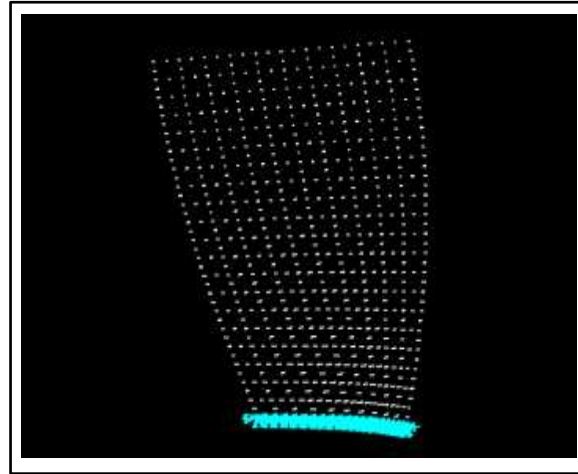


Fig. 2. Front view of the constrained root of the turbine blade

2.2. The contour plots

The solutions are obtained from the post-process, after the pre-processing of the first model. The numerical calculations are performed by finite element method using ANSYS software based on the Block Lanczos method. In general, post-processing includes a variety of results in the form of a list, contour plots, vector plots, or animations as per the requirement. The results are further obtained for the element removal (starting from 0 to 4)

for five different models. Here, the solutions of stress distribution are demonstrated in the form of contour plots. These plots highlight the distribution of stress, displacement, temperatures, and other parameters on the model geometry in an effective way. The contour plot for Von Mises stresses distribution is extracted as shown in Fig. 3. Further, the solution in the form of contour plots for five different models is extracted and presented in the later section.

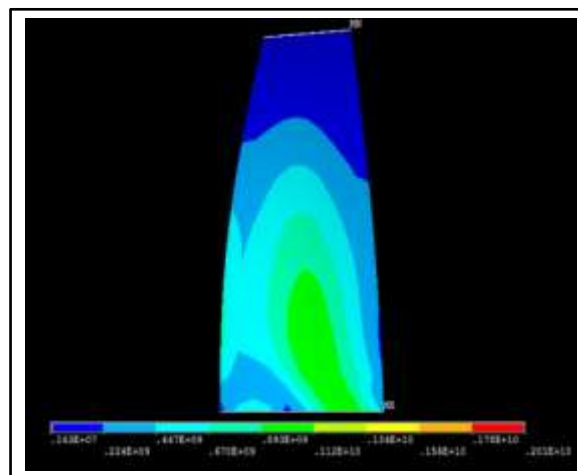


Fig. 3. Von Mises stresses distribution.

2.3. Element removal (crack formation) in the turbine blade model

In the current work, five different models are analyzed for the behavior of natural frequency and stress distribution under 10 modes of vibration, in which the sequence of a) ER=0, b) ER=1, c) ER=2, d) ER=3, and e) ER=4 is followed for each mode of vibration. Then, the results are formulated by re-

performing the procedure as described earlier. Furthermore, the results obtained from all five models are collectively analyzed to conclude in the later section. The validation is then performed, by comparing the resultant stiffness (due to the crack formation) to the actual stiffness of the blade (in the absence of the crack). The single element removed from the turbine blade model is shown in Fig. 4.

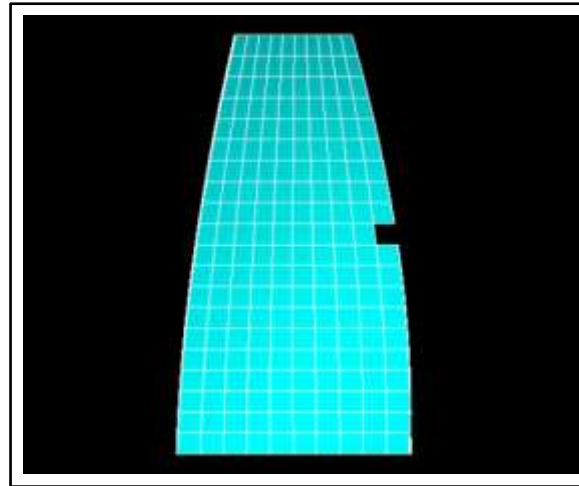


Fig. 4. Turbine blade model with one element removed

3. Results and discussion

The natural frequency and the stress concentration are the key parameters for the model analysis of the turbine blades. From the operation point of view in the industrial sector, prior data about the natural frequency is significant, because when the blades are excited through different dynamic loads, there strongly exists a chance of resonance if the excited frequency matches with one of the natural frequencies of the blade or the excitation shape match the mode shape of the blade [30]. Therefore, the resonance can lead to a higher amplitude of vibrations, which is highly undesirable for the better operating life of the machinery. For this reason, it is of much importance to predict and determine the natural frequencies and mode shapes of the blade. Moreover, the stress distribution/concentration is also important, because it gives a quantitative approach to observe which zone is undergoing a maximum and minimum stress concentration under loading conditions. Therefore, the natural frequency and stress distribution of the

gas turbine blade are analyzed from the finite element-based method. The results are obtained for five different model analyses of a turbine blade at different element removal (starting from 0 to 4). Initially, no element is removed to obtain the normal stress distribution and natural frequency of 10 mode points for the sake of reference. Subsequently, one element is removed from the model, and natural frequency and stress concentration are re-formulated for ten different modes. The process is repeated up to four elements removal in sequential order.

3.1. Mode shapes for stress analysis

A mode shape and a modal frequency are two characteristics of a vibration mode. It is assigned a number based on the number of half-waves in the vibration. In the first part of the blade analysis, the stress distributions are presented in the form of mode shapes. The mode shapes represent the stress distribution in thermal as well as radial stresses that can be observed in the turbine blade. Moreover, the results for 10 mode shapes are presented for

stress distribution under sequential crack generation. The results of mode-1 are represented in Fig. 5. It can be seen that a higher stress concentration is observed at the

root of the blade before the crack formation. As the crack initiates in the form of material removal, the maximum stress concentration gradually propagates toward the crack zone.

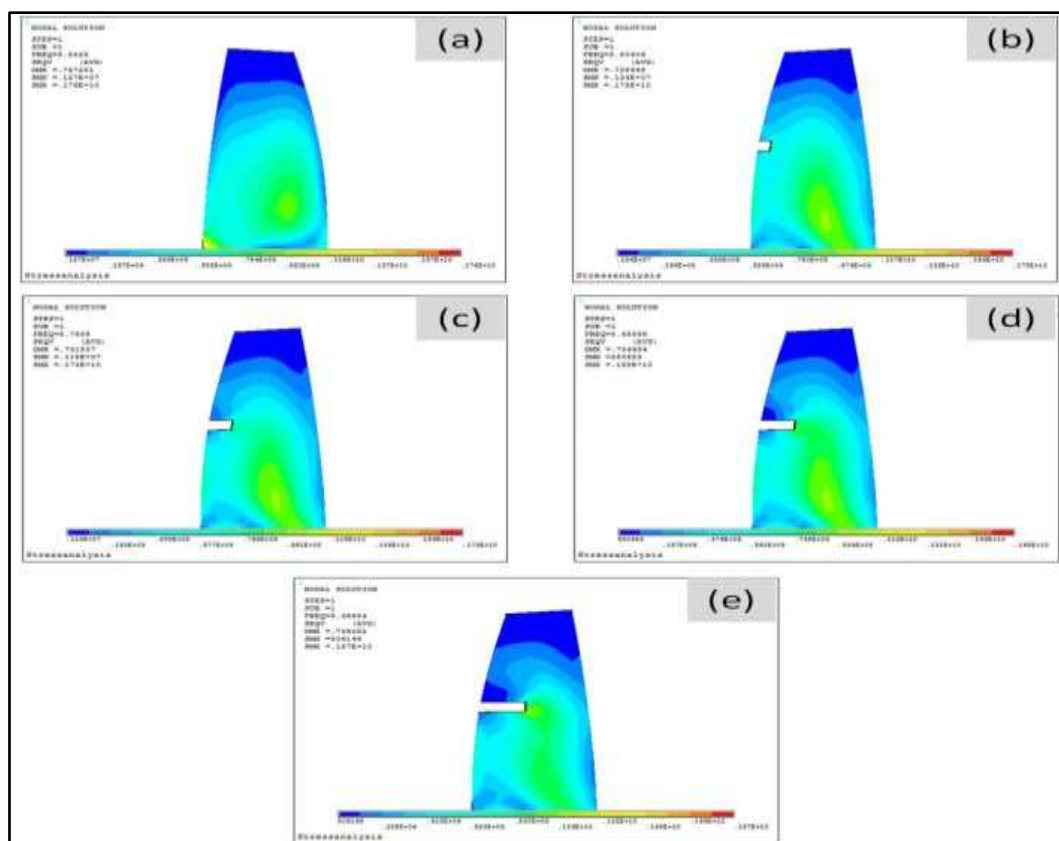


Fig. 5. Mode Shapes for Node 1 (a) ER=0, (b) ER=1 (c) ER=2, (d) ER=3, (e) ER=4

The results of mode-2 are highlighted in Fig. 6. The maximum stress concentration is also observed on the root of the blade for mode-2 in case of no crack formation. However, it can be seen that the higher stress concentration is fairly detected around the crack zone when crack formation proceeds towards the third and fourth element removal. Moreover, it is pertinent to highlight that the value of maximum stress increases, as the mode of vibration increases for each particular element removal. It is important to highlight that, with the increase in the modes of vibration, the stress distribution zone gradually contracts nearly around the crack zone. But the value of maximum stress concentration gradually increases, upon the increase in the mode of vibrations. Moreover, the maximum value is also observed closer to the crack area near the

tip of the blade. This trend can be seen in Fig. 7. Furthermore, the counterplots for the fourth mode of vibration are represented in Fig 8. The plots also exhibit a similar trend as observed earlier. As expected, the maximum stress value is increased compared to the preceding mode of vibration. Additionally, it is important to highlight that, the maximum stress value seems to be shifted closer to the tip of the blade in case of larger crack formation. Moreover, the fifth mode shape results are represented in Fig. 9. In this, the stress concentration is low for no crack formation and thus the value gradually increases with the increase in crack propagation. Whereas, the overall maximum stress value is higher due to the large mode of vibration as compared to the preceding modes for all cases.

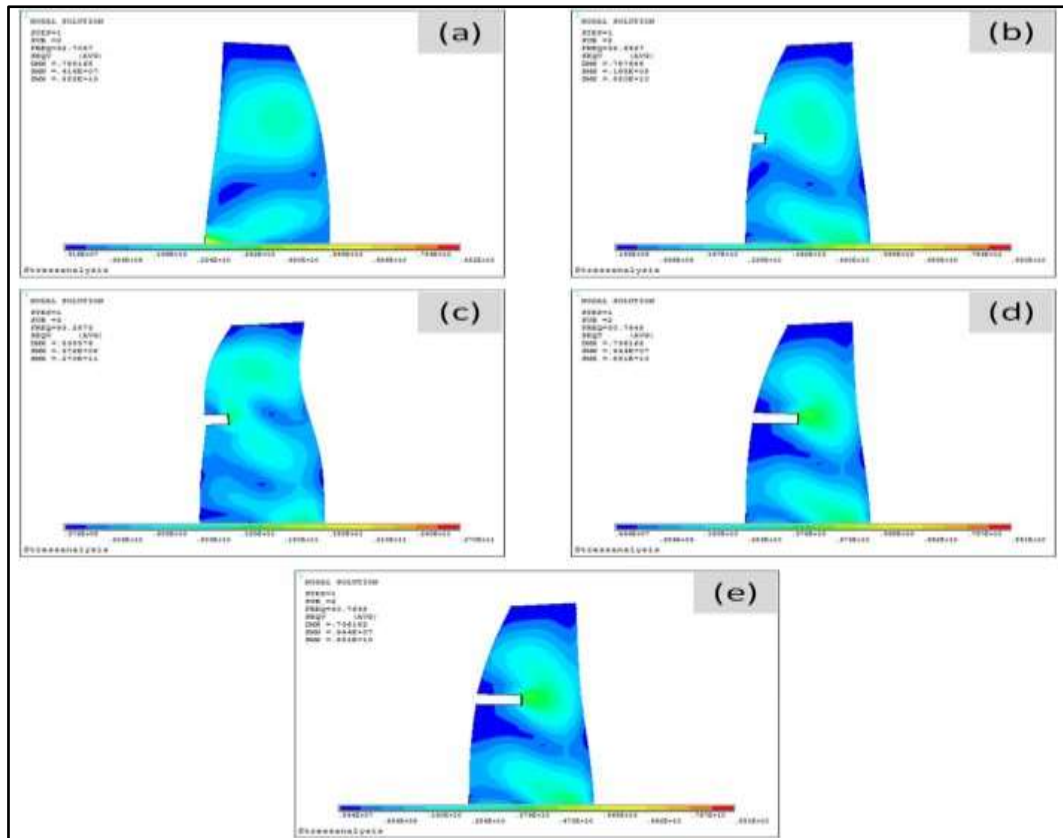


Fig. 6. Mode Shapes for Node 2 (a) ER=0, (b) ER=1 (c) ER=2, (d) ER=3, (e) ER=4

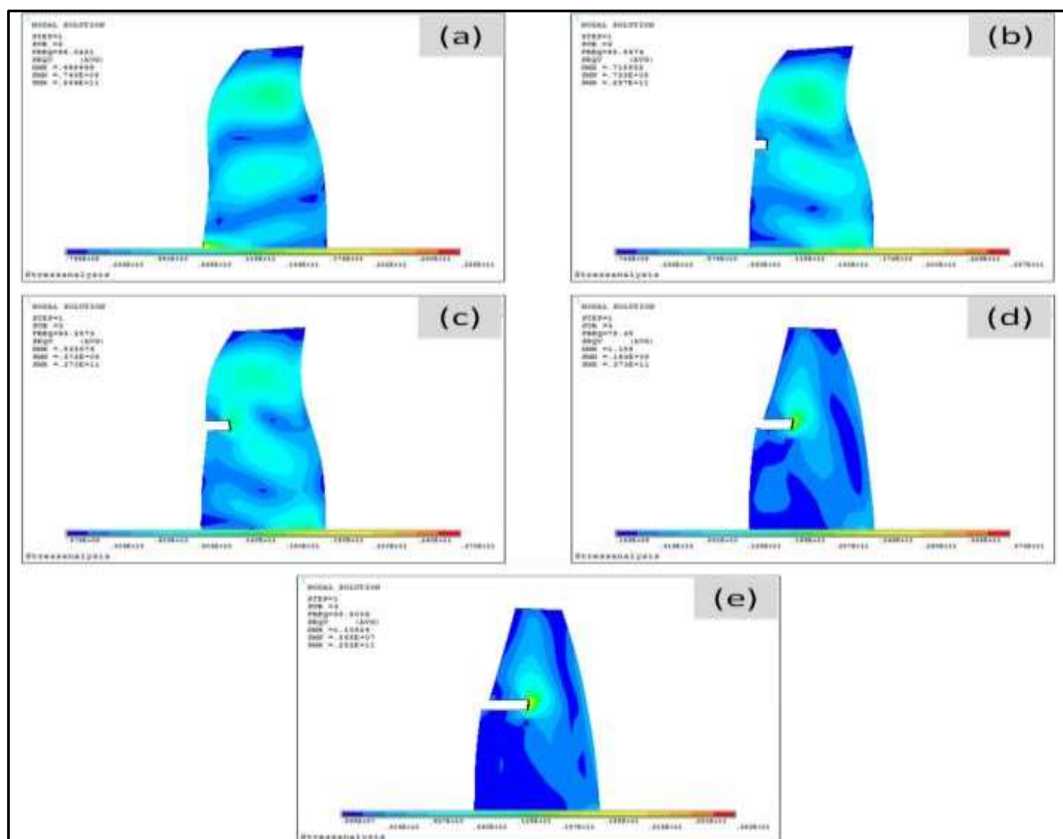


Fig. 7. Mode Shapes for Node 3 (a) ER=0, (b) ER=1 (c) ER=2, (d) ER=3, (e) ER=4

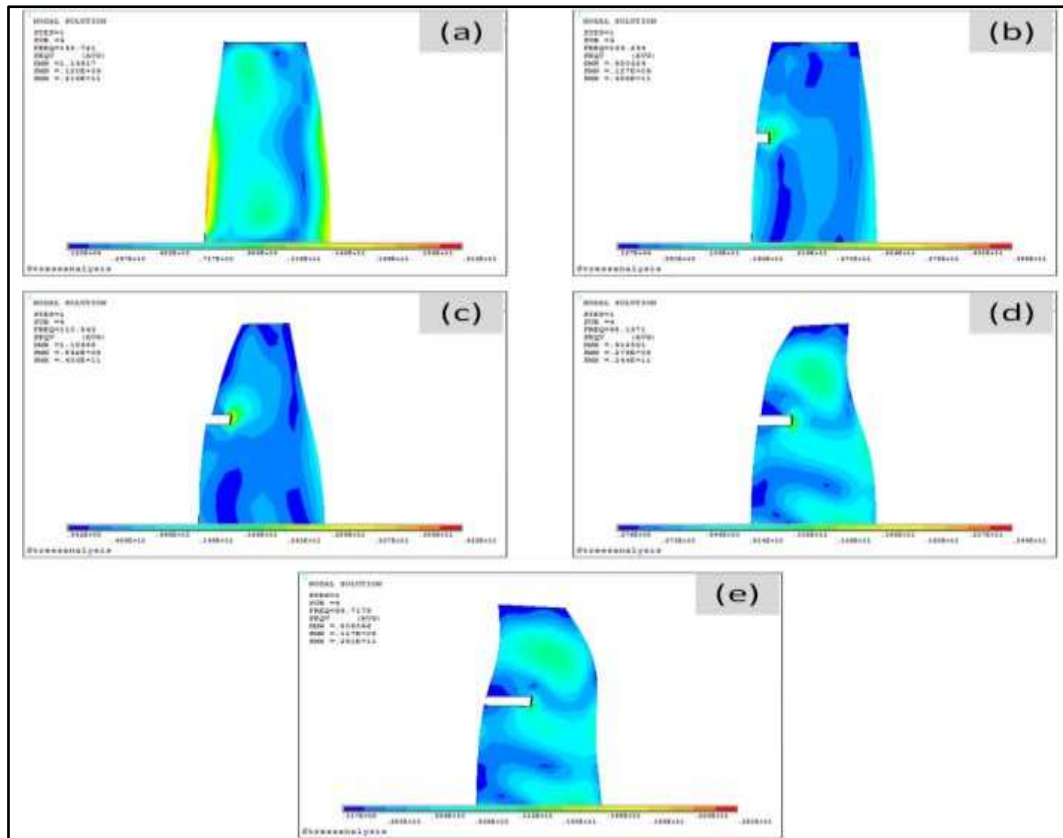


Fig. 8. Mode Shapes for Node 4 (a) ER=0, (b) ER=1 (c) ER=2, (d) ER=3, (e) ER=4

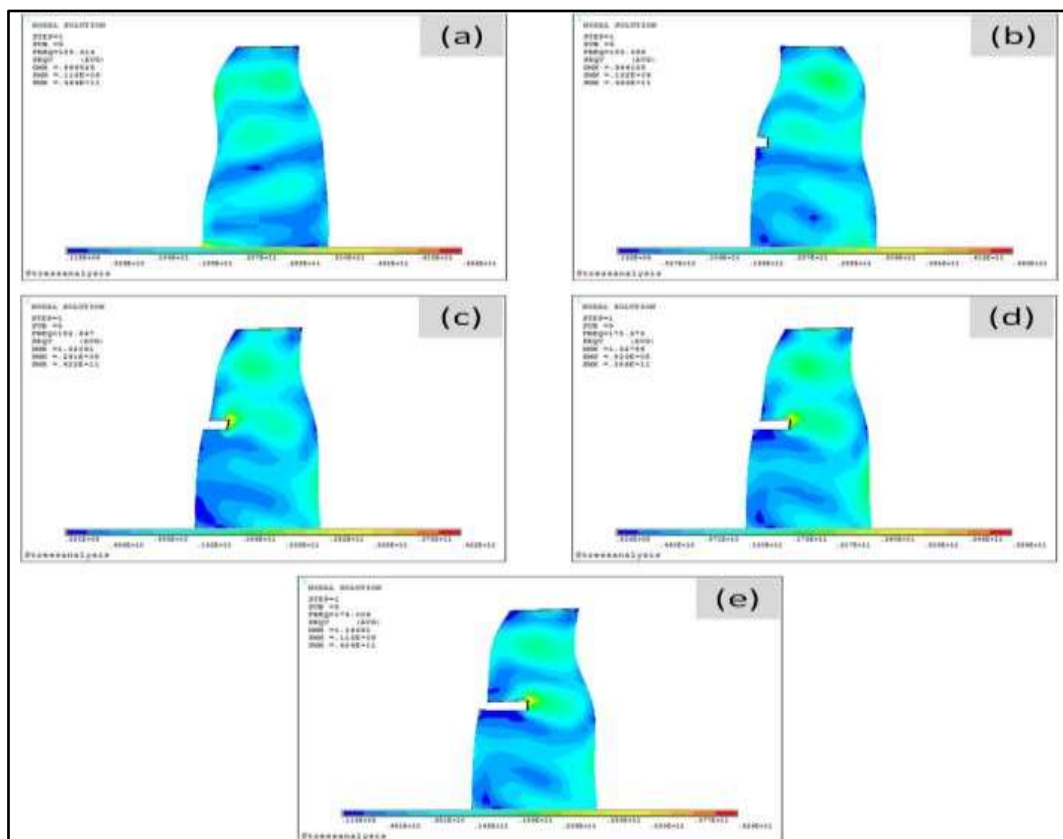


Fig. 9. Mode Shapes for Node 5 (a) ER=0, (b) ER=1 (c) ER=2, (d) ER=3, (e) ER=4

Fig. 10 highlights that, the trend for mode shape 6 is diverse as compared to the previous modes. In this mode of vibration, a large stress concentration value can be seen at the tip of the blade. Therefore, it is evident, that the high modes of vibration impact larger stresses, which is extremely undesirable, because it can

lead to the failure of the turbine blade. Under these conditions, crack formation is another factor that drastically influences stress concentration. Moreover, at times the large stress concentration at the upper region alongside the blade is also observed in the higher modes.

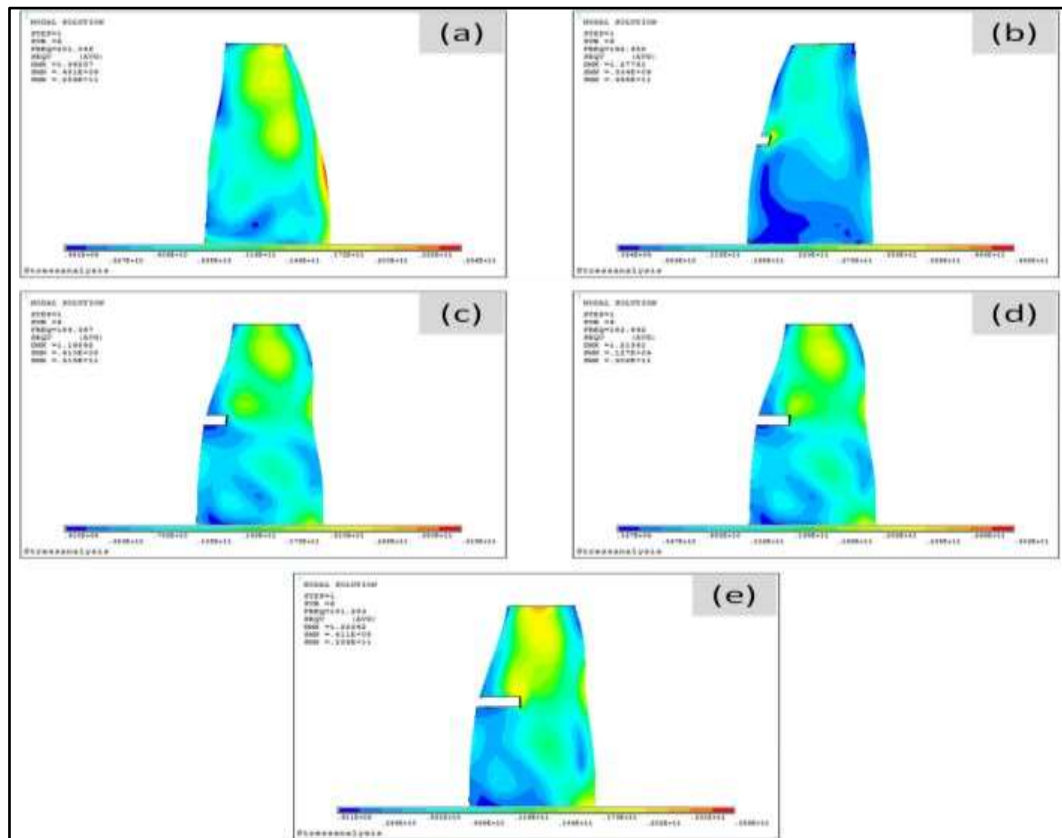


Fig. 10. Mode Shapes for Node 6 (a) ER=0, (b) ER=1 (c) ER=2, (d) ER=3, (e) ER=4

The gradual increase in the number of modes reflects the abnormal behavior of the turbine blade due to the reason that more stresses are generated when both the factors i.e., modes of vibration and crack propagation increase. Moreover, the model also shows deformation under these circumstances which can be seen in Fig. 11, Fig. 12, Fig. 13, and Fig. 14 for mode shapes 7, 8, 9, and 10, respectively. The mode shapes show that for low modes of vibration, a substantial amount of stress and strain is measured at the roots of the turbine blade. Furthermore, it can be shown that the material anomaly alters the stress distribution across the blade's profile. It's worth noting that the stresses are fairly concentrated adjacent to

the blade roots when the analysis is performed without crack formation. However, as one element is eliminated (formation of a crack zone), the stress concentration begins to shift toward the crack zone at the blade's trailing edge. The high-stress concentration occurs at the zone of the blade where the crack originates, as seen by this trend [31]. The more the crack develops, the greater the stress concentration near the material abnormality zone, resulting in blade failure. The higher mode forms of the turbine blades clearly show this trend.

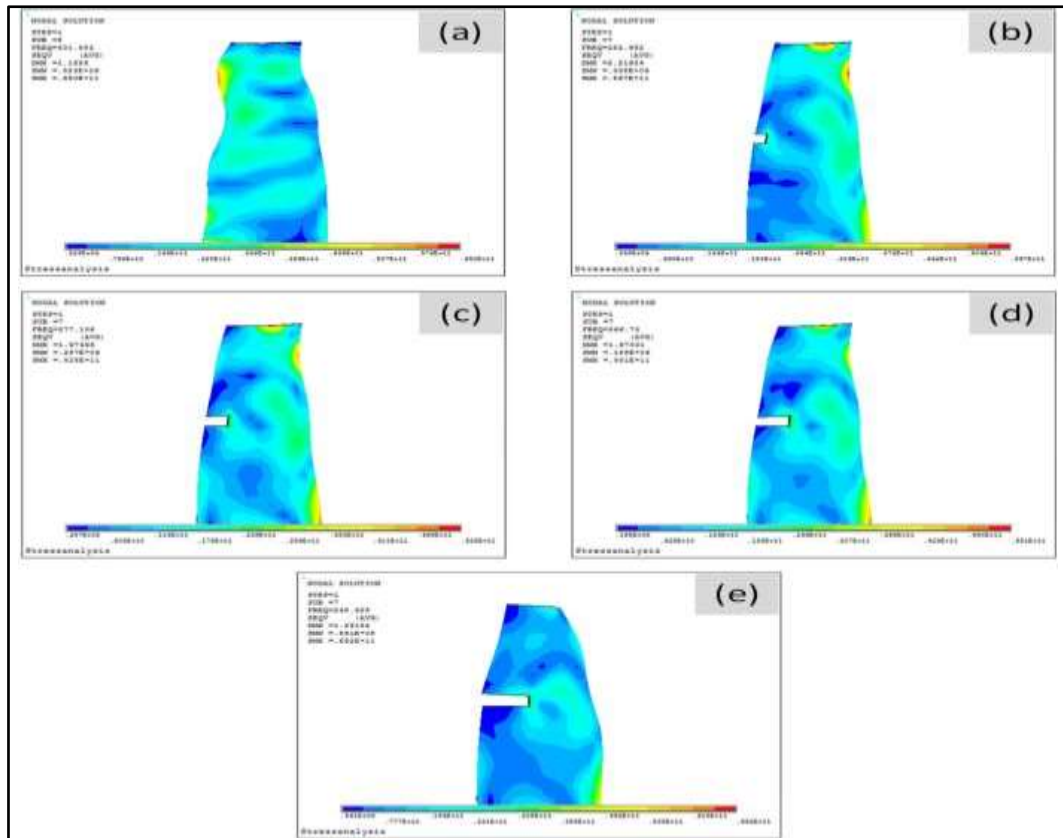


Fig. 11. Mode Shapes for Node 7 (a) ER=0, (b) ER=1 (c) ER=2, (d) ER=3, (e) ER=4

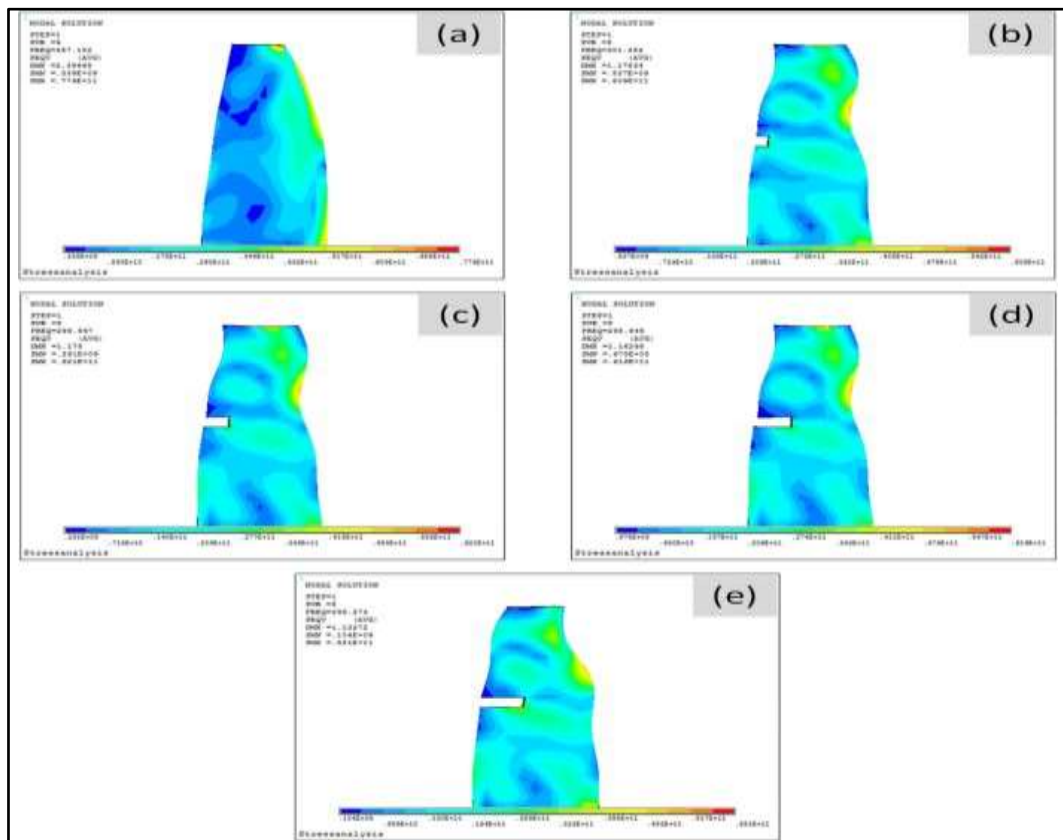


Fig. 12. Mode Shapes for Node 8 (a) ER=0, (b) ER=1 (c) ER=2, (d) ER=3, (e) ER=4

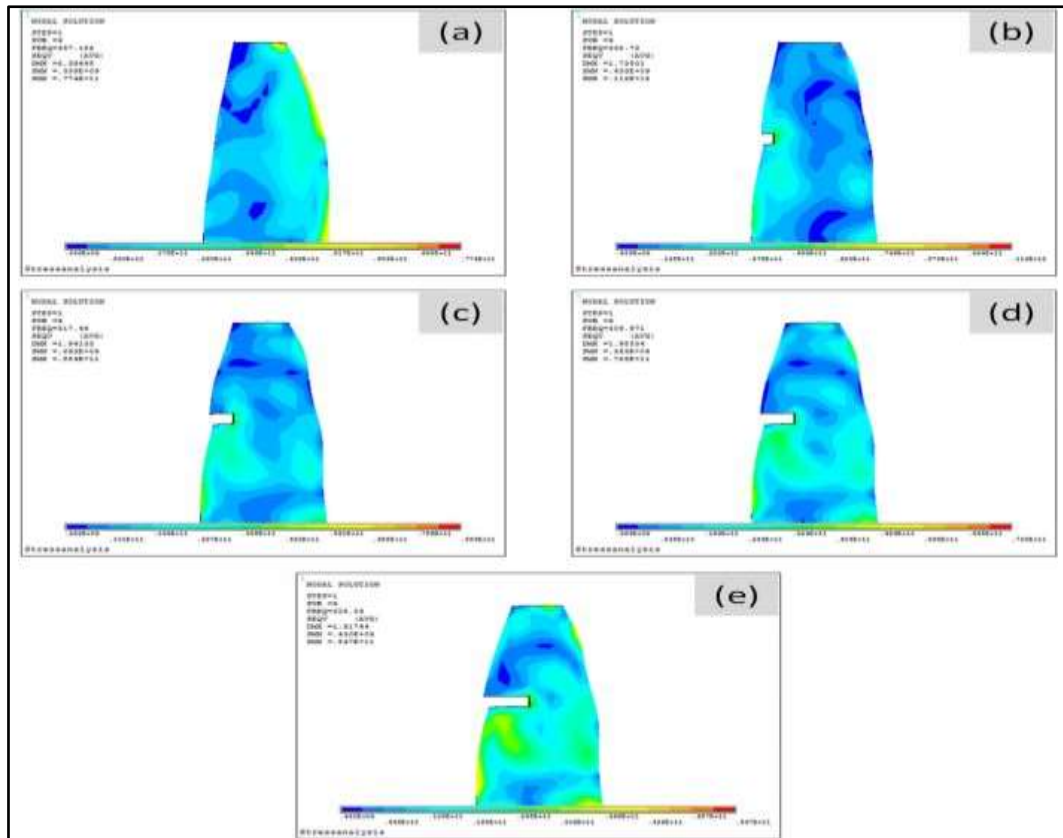


Fig. 13. Mode Shapes for Node 9 (a) ER=0, (b) ER=1 (c) ER=2, (d) ER=3, (e) ER=4

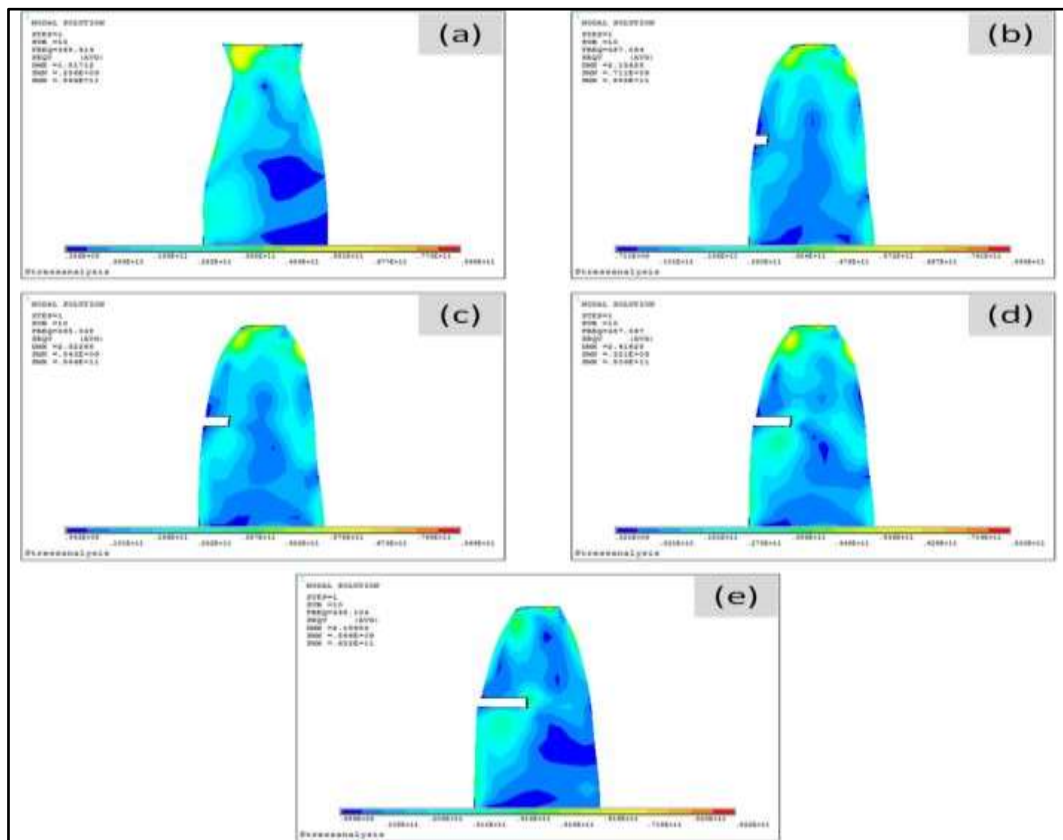


Fig. 14. Mode Shapes for Node 10 (a) ER=0, (b) ER=1 (c) ER=2, (d) ER=3, (e) ER=4

3.2. Variation of natural frequency and stress concentration

Finally, the analysis of natural frequency and stress concentration (maximum and average) are represented graphically for better illustration and to provide conclusive findings for five different element removal under 10 mode shapes. Fig.15, represents the variation of natural frequency, maximum stress concentration, and average stress concentration for modes (1 and 2). It can be seen that the natural frequency follows a decreasing trend as the crack propagates. This is because the crack formation directly impacts the material stiffness properties. Although the variation of natural frequency is not so significant for the first two modes in terms of element removal, it can be seen that the natural frequency

collectively goes at a higher level for mode-2, as compared to mode-1. The minimum and maximum values for the natural frequency of the blade are around (8.46 - 8.82) Hz for mode-1 and (30.7 - 32.7) Hz in the case of mode-2, respectively. The maximum stress concentration is located mostly on the root of the blade for the low modes of vibration. Moreover, the average and maximum stress concentration firstly increases as the crack propagates, then decreases. This trend is observed due to the material behavior of the alloy steel. For mode-1, the stress variation is not so significant as well, due to the low mode of vibration. For mode-1 and mode-2, the maximum observed values of stress concentration are 0.98 GPa, and 9.03 GPa, respectively.

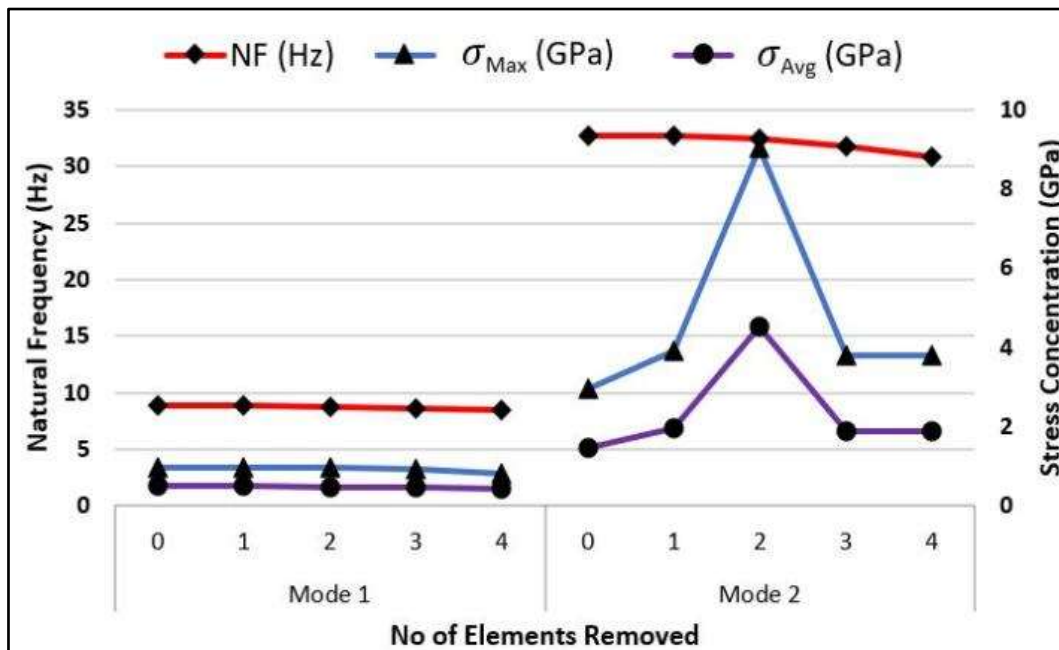


Fig. 15. Variation of NF and SC along element removed for mode (1-2)

As the mode of vibration increases, the steepness of the natural frequency curve also increases. Moreover, the stress concentration follows the same trend of steepness as the natural frequency at a relatively higher stress concentration bandwidth. This trend can be significantly observed in Fig. 16. The minimum and maximum observed values of natural

frequency for mode-3 and mode-4 are around (58.5 - 96) Hz and (95.7 - 143.7) Hz, respectively. Whereas the maximum stress concentration for mode-3 and mode-4 is 16.6 GPa, and 24.1 GPa, respectively. Whereas, the average stress concentration gives the overall stress value for the entire blade.

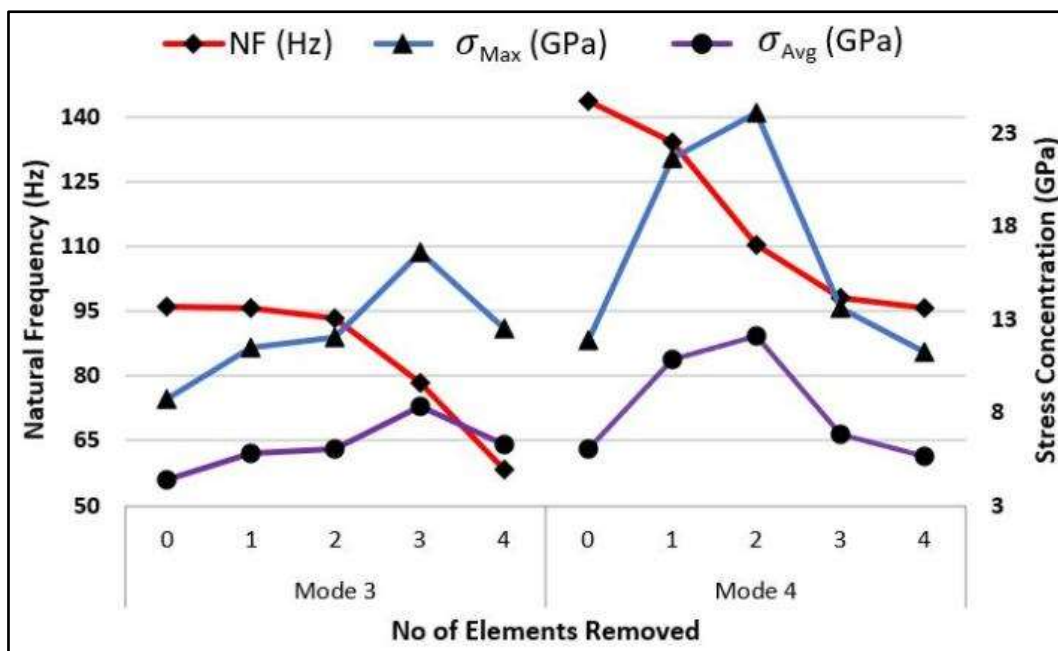


Fig. 16. Variation of NF and SC along element removed for mode (3-4)

Furthermore, the variation of natural frequency and stress concentration for mode-5 and 6 are presented in Fig. 17. Here the minimum and maximum values of natural frequency for mode-5 and 6 are around (174 - 185.3) Hz and (181.2 - 201) Hz, respectively. The natural frequency decreases upon

sequential element removal. Moreover, the maximum stress concentration for mode-5 and 6 are around 25.8 GPa and 27.2 GPa, respectively. It is pertinent to highlight that, the maximum SC value is observed near the tip of the blade for higher modes, as discussed earlier.

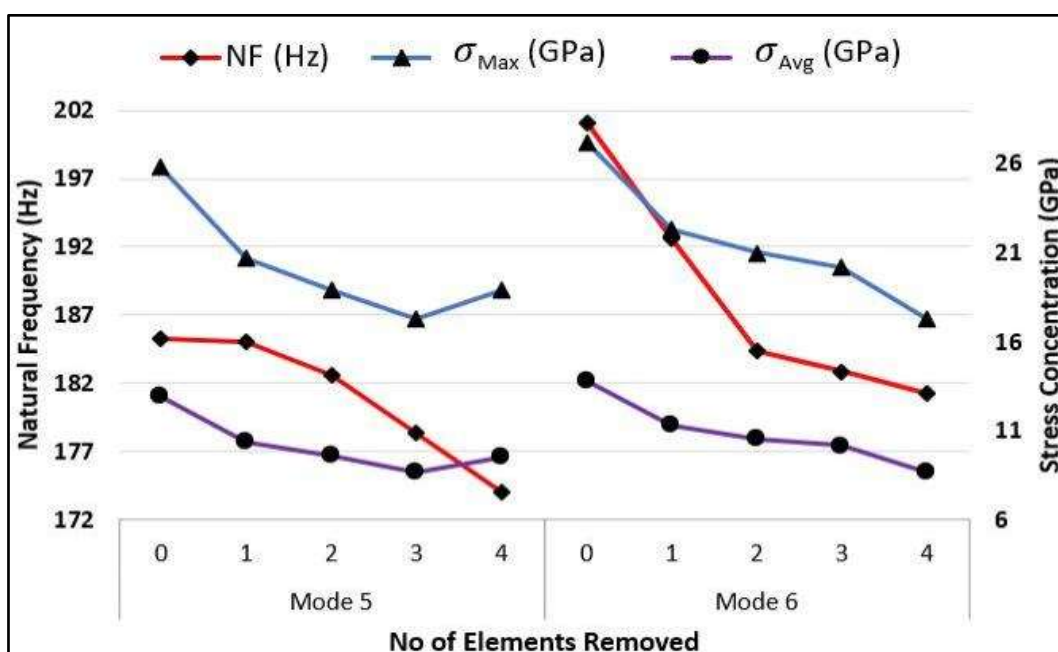


Fig. 17. Variation of NF and SC along element removed for mode (5-6)

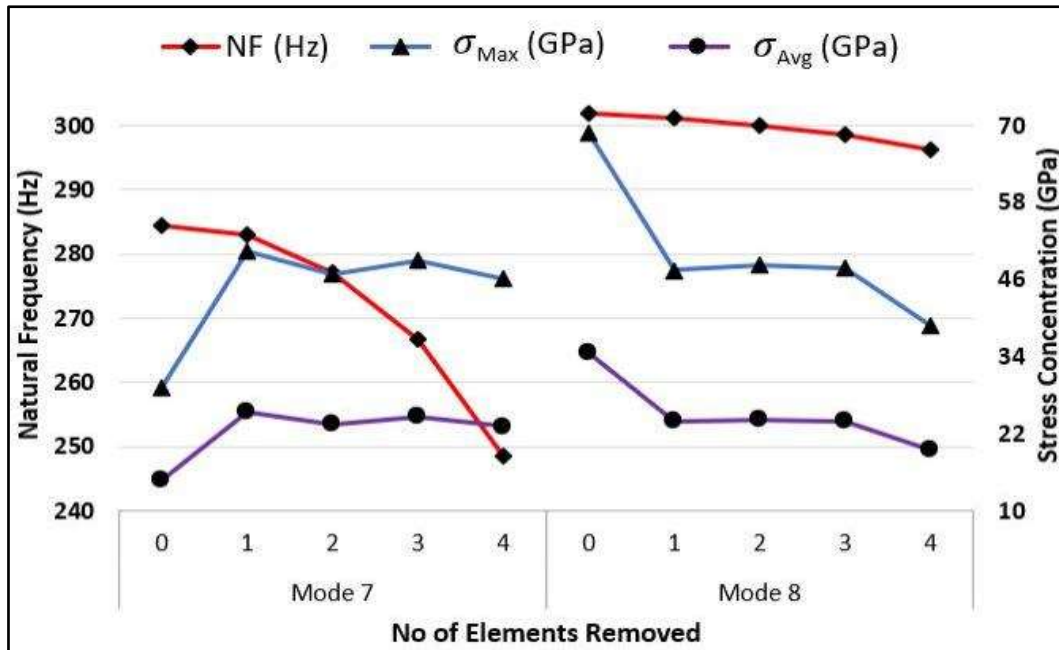


Fig. 18. Variation of NF and SC along element removed for mode (7-8)

Fig. 18 highlights the trend of natural frequency and stress concentration for mode (7-8). The minimum and maximum values of natural frequency for mode-7 and mode-8 are observed to be (248.6 - 284.4) Hz and (296.2 - 301.8) Hz, respectively. The overall increasing value of the natural frequency with the increase

in the mode of vibration and the decreasing trend upon each material removal for a particular mode can also be seen. Moreover, the maximum stress concentration values for mode 7 and mode 8 are around 50.4 GPa and 68.8, respectively, which is comparatively higher than the previous modes.

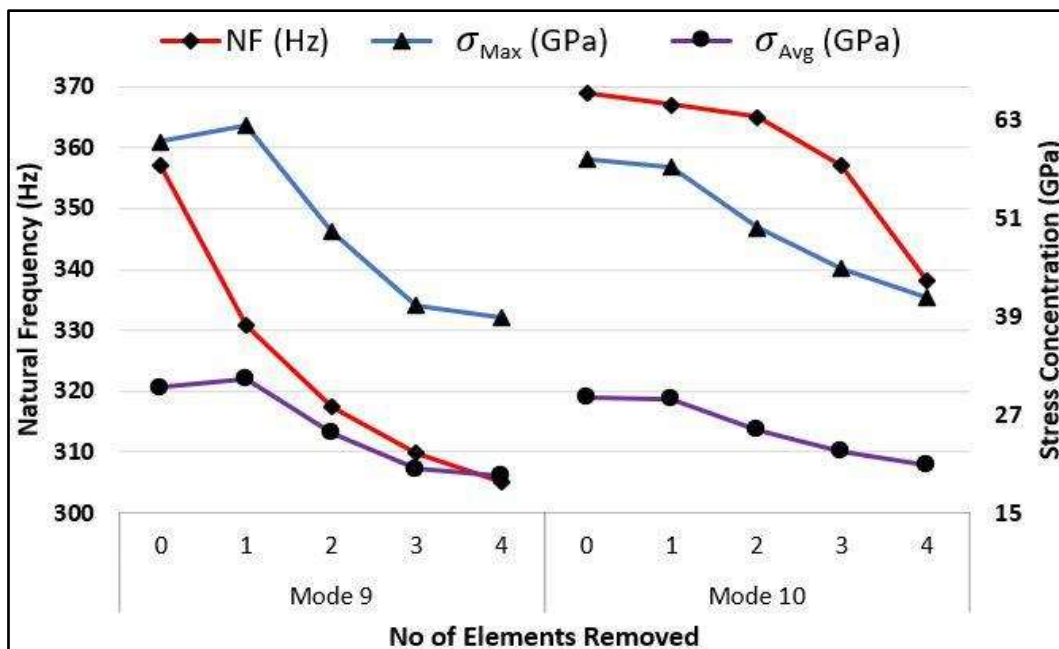


Fig. 19. Variation of NF and SC along element removed for mode (9-10)

Similarly, the stress concentration goes up to its maximum value for mode-9 and 10.

Whereas, the natural frequency also exhibits this trend. Moreover, a higher gradient is

observed in both parameters. This is because of the material behaviors abnormally under higher mode and greater crack propagation. The minimum and maximum observed values of natural frequency for mode-9 and 10 are around (305 - 357) Hz and (338 - 369) Hz, respectively. Whereas, the maximum values of the stress concentration for mode-9 and 10 are 62.3 GPa and 58.1 GPa, respectively. Moreover, the

percentage decrease of the natural frequency for all 10 modes is summarized in Table. 2, in the form of a percentage decrease for a better reflection of the overall trend. Moreover, the percentage decrease further represents a quantitative measure, of to what extent the observed values of natural frequency are deviating from their preceding values.

Table 2. Summary of the percentage decrease in the NF of blade

Mode of Vibrations	Percentage decrease in NF (Hz)			
	ER (0-1)	ER (1-2)	ER (2-3)	ER (3-4)
Mode-1	0.21	0.54	1.14	2.19
Mode-2	0.16	0.70	1.85	3.32
Mode-3	0.39	2.46	15.97	25.36
Mode-4	6.59	17.6	11.22	2.46
Mode-5	0.12	1.30	2.34	2.44
Mode-6	4.17	4.30	0.80	0.88
Mode-7	0.52	2.07	3.74	6.78
Mode-8	0.20	0.44	0.43	0.79
Mode-9	7.40	4.01	2.35	1.59
Mode-10	0.50	0.55	2.18	5.31

It is important to understand how the natural frequency (NF) fluctuates with the number of elements removed, which is presumed to represent the crack size in this instance. To pursue this perspective, a relationship was developed between the natural frequency ratio and the number of elements removed for the first three modes as shown in Fig. 20. It is observed that as the number of elements removed increases the natural frequency decreases. These results are consistent with the ones already presented in Lui and Zhu's research [32] that are also plotted in Fig. 20 for the dynamic model of a cantilever

beam for the first three normalized mode shapes of the cracked cantilever beam. In this research, the crack size is defined as

$$\text{Crack size} = \frac{X_1}{L} \times \frac{h_1}{h} \times \frac{L_2}{L} \quad (1)$$

Where X_1 is the crack's endpoint distance, h_1 is the crack's depth from the top, L_2 is the crack length, h is the cantilever beam's height and L is the length of the cantilever beam. The crack was studied with and without local flexibilities (LF). The current experiment and Lui and Zhu's research both reveal the same response against the natural frequency ratio, as illustrated in Fig. 20.

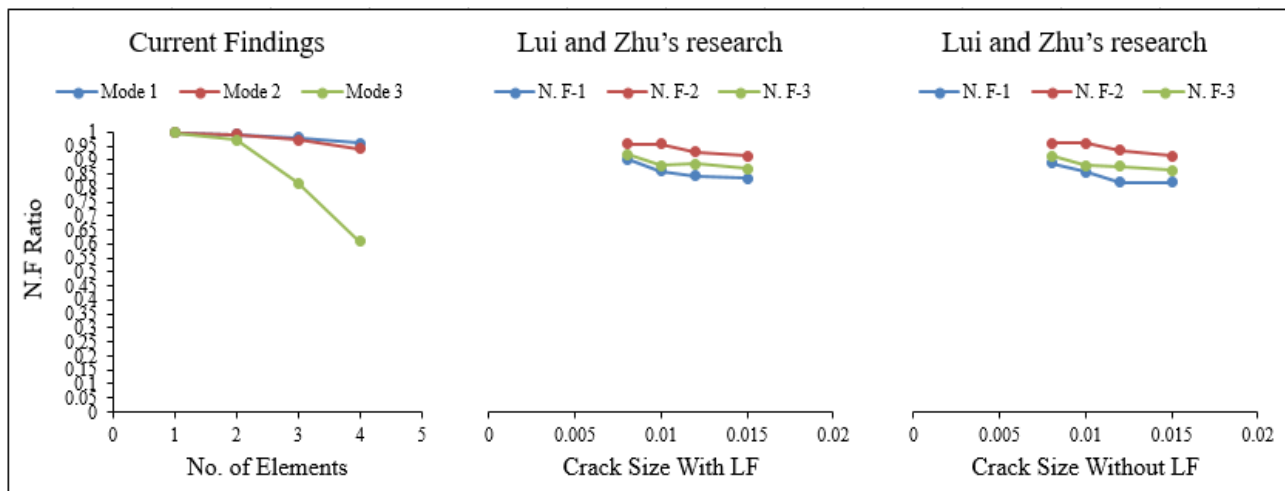


Fig. 20. Comparison of current results with Lui and Zhu

4. Conclusion

In this study, a comprehensive analysis has been carried out through five different models under sequential element removal (from 0 to 4) and ten modes of vibration to study the behavior of natural frequency and stress distribution of the gas turbine blade. In this regard, the modal analysis technique gives a close approximation to the actual behavior of the turbine blade in operation under loading conditions. The crack formation through material removal in the FEA model of the turbine blade is used for SC and NF analysis, as the sequential removal of each element is analogous to the decrease in the stiffness of the system. Moreover, the extracted mode shapes through model analysis fairly describe the relative stress distribution over the blade geometry. Some key conclusions can be drawn based on the five different models as follows;

- The element removal, also known as crack creation, causes the natural frequency of the gas turbine blade to be affected. The natural frequency will decrease as the number of elements removed, increases. The natural frequency of the blade is undoubtedly influenced by the stiffness of the blade's material, which varies as the blade's mass decreases as a result of crack formation.
- As the mode of vibration increases, so does the natural frequency. The natural frequency of the blade has a low value for the lower mode of vibration and a high value for the higher mode of vibration. This presentation

will aid with blade pre-design to prevent resonance complications.

- At the root of the gas turbine blade, there is a large concentration of stress. Because of the element removal, the stress concentration is pushed toward the blade's tip, and it reaches a high value around the crack in the blade. This is a terrifying act that results in the blade's utter failure.
- The stress concentration increases dramatically when the mode of vibrations changes. For a low mode of vibration, the stress concentration is fairly dominant towards the root of the blade, but when both crack formation and mode of vibration rise, the stress concentration eventually shifts towards the fracture zone near the tip of the blade.
- In a nutshell, when the mode of vibrations is increased sequentially, both natural frequency and stress concentration rise in value.

Declarations:

Funding

The authors did not receive support/funding from any organization for the submitted work.

Availability of data and materials

The data used to support the findings of this study are available from the corresponding author upon request.

Competing interests

The authors have no competing interests to declare that are relevant to the content of this article.

References

- [1] O. Kauss, K. Naumenko, G. Hasemann, and M. Krüger, "Structural Analysis of Gas Turbine Blades Made of Mo-Si-B Under Stationary Thermo-Mechanical Loads," in *Advances in Mechanics of High-Temperature Materials*, ed: Springer, 2020, pp. 79-91.
- [2] S. Bornassi, M. Ghalandari, and S. F. Maghrebi, "Blade synchronous vibration measurements of a new upgraded heavy duty gas turbine MGT-70 (3) by using tip-timing method," *Mechanics Research Communications*, vol. 104, p. 103484, 2020.
- [3] J. Zeng, K. Chen, H. Ma, T. Duan, and B. Wen, "Vibration response analysis of a cracked rotating compressor blade during run-up process," *Mechanical Systems and Signal Processing*, vol. 118, pp. 568-583, 2019.
- [4] J. Rodríguez, L. Castro, A. Tejada, J. García, J. Rodríguez, E. Galindo, *et al.*, "Fatigue of steam turbine blades at resonance conditions," *Engineering Failure Analysis*, vol. 104, pp. 39-46, 2019.
- [5] Z. Mazur, A. Luna-Ramirez, J. Juárez-Islas, and A. Campos-Amezcuca, "Failure analysis of a gas turbine blade made of Inconel 738LC alloy," *Engineering failure analysis*, vol. 12, pp. 474-486, 2005.
- [6] S. Rani, A. Agrawal, and V. Rastogi, "Vibration analysis for detecting failure mode and crack location in first stage gas turbine blade," *Journal of Mechanical Science and Technology*, vol. 33, pp. 1-10, 2019.
- [7] B. Ross, C. Wells, C. Schoof, and C. Lange, "Analysis of multiple gas turbine failures due to high order (6e) resonant vibrations," *Technology, Law and Insurance*, vol. 3, pp. 33-45, 1998/03/01 1998.
- [8] A. Rahmani, G. Eslami, and R. Soleimani, "Thermo-Mechanical Fatigue (TMF) Life Prediction in Gas Turbine Blades," *Life Science Journal*, vol. 10, 2013.
- [9] C. B. Meher-Homji and G. Gabriles, "Gas Turbine Blade Failures-Causes, Avoidance, And Troubleshooting," in *Proceedings of the 27th turbomachinery symposium*, 1998.
- [10] M. P. Boyce, *Gas turbine engineering handbook*: Elsevier, 2011.
- [11] R. Viswanathan, "An investigation of blade failures in combustion turbines," *Engineering Failure Analysis*, vol. 8, pp. 493-511, 2001.
- [12] B. Swain, P. Mallick, S. Patel, R. Roshan, S. Mohapatra, S. Bhuyan, *et al.*, "Failure analysis and materials development of gas turbine blades," *Materials Today: Proceedings*, 2020.
- [13] N. P. Pature, M. Gell, and E. H. Jordan, "Thermal barrier coatings for gas-turbine engine applications," *Science*, vol. 296, pp. 280-284, 2002.
- [14] R. Nakajima, H. Katori, M. Arai, and K. Ito, "Comprehensive Numerical Simulation on Thermally Grown Oxide and Internal Stress Evolutions in Thermal Barrier Coatings," in *Key Engineering Materials*, 2020, pp. 343-348.
- [15] M. Rajabinezhad, A. Bahrami, M. Mousavinia, S. J. Seyedi, and P. Taheri, "Corrosion-Fatigue Failure of Gas-Turbine Blades in an Oil and Gas Production Plant," *Materials*, vol. 13, p. 900, 2020.
- [16] E. Poursaeidi, M. Aieneravaie, and M. Mohammadi, "Failure analysis of a second stage blade in a gas turbine engine," *Engineering failure analysis*, vol. 15, pp. 1111-1129, 2008.
- [17] N. Eliaz, G. Shemesh, and R. Latanision, "Hot corrosion in gas turbine components," *Engineering failure analysis*, vol. 9, pp. 31-43, 2002.
- [18] N. Vardar and A. Ekerim, "Failure analysis of gas turbine blades in a thermal power plant," *Engineering Failure Analysis*, vol. 14, pp. 743-749, 2007.
- [19] R. Ebara, "Corrosion fatigue crack initiation in 12% chromium stainless steel," *Materials Science and Engineering: A*, vol. 468, pp. 109-113, 2007.
- [20] M. Arai and T. Suidzu, "Porous ceramic coating for transpiration cooling of gas turbine blade," *Journal of Thermal Spray Technology*, vol. 22, pp. 690-698, 2013.
- [21] B. Rottwinkel, C. Nölke, S. Kaierle, and V. Wesling, "Crack repair of single crystal turbine blades using laser cladding technology," *Procedia Cirp*, vol. 22, pp. 263-267, 2014.
- [22] D. Davidov and A. Ermakov, "Blade wave finite element," *Research Journal of Applied Sciences*, vol. 9, pp. 849-854, 2014.

- [23] R. Loewy and N. Khadert, "Structural dynamics of rotating bladed-disk assemblies coupled with flexible shaft motions," *AIAA Journal*, vol. 22, pp. 1319-1327, 1984.
- [24] S. Ghoreishi, M. Salari, S. Pourhosseini, and A. Bahmani, "Experimental and numerical modal analysis of the first and second stage compressor blades," *Engineering Solid Mechanics*, vol. 7, pp. 341-354, 2019.
- [25] J.-C. Chang, Y.-H. Yun, C. Choi, and J.-C. Kim, "Failure analysis of gas turbine buckets," *Engineering Failure Analysis*, vol. 10, pp. 559-567, 2003/10/01/ 2003.
- [26] G. L. Forbes and R. B. Randall, "Estimation of turbine blade natural frequencies from casing pressure and vibration measurements," *Mechanical Systems and Signal Processing*, vol. 36, pp. 549-561, 2013.
- [27] A. Rahmani, A. Ghanbari, and A. Mohammadi, "Experimental modal analysis of a first stage blade in ALSTOM gas turbine," in *Applied Mechanics and Materials*, 2014, pp. 303-307.
- [28] C. Li, Z. Shen, B. Zhong, and B. Wen, "Study on the Nonlinear Characteristics of a Rotating Flexible Blade with Dovetail Interface Feature," *Shock and Vibration*, vol. 2018, 2018.
- [29] T. Takahashi, K. Watanabe, and T. Takahashi, "Thermal conjugate analysis of a first stage blade in a gas turbine," in *ASME Turbo Expo 2000: Power for Land, Sea, and Air*, 2000.
- [30] A. Presas, D. Valentin, C. Valero, M. Egusquiza, and E. Egusquiza, "Experimental Measurements of the Natural Frequencies and Mode Shapes of Rotating Disk-Blades-Disk Assemblies from the Stationary Frame," *Applied Sciences*, vol. 9, 2019.
- [31] E. Poursaeidi, A. Babaei, M. M. Arhani, and M. Arablu, "Effects of natural frequencies on the failure of R1 compressor blades," *Engineering Failure Analysis*, vol. 25, pp. 304-315, 2012.
- [32] J. Liu, W. Zhu, P. Charalambides, Y. Shao, Y. Xu, and X. Fang, "A dynamic model of a cantilever beam with a closed, embedded horizontal crack including local flexibilities at crack tips," *Journal of Sound and Vibration*, vol. 382, pp. 274-290, 2016.